SUPPLEMENTARY METHODS

Cell Line Development and Maintenance

BCaP cell lines were derived in the Ricke lab as previously described[1]. Briefly, a single cell taken from a benign human prostate, and was immortalized with T-antigen (BPH1 cell line). Xenografts using the BPH1 cell line and rodent urogenital mesenchyme were implanted under the kidney capsule of mice that were either untreated or treated with testosterone and estradiol. In untreated mice, the BPH1 xenograft did not form a tumor, and cells isolated from this xenograft are the $BCaP^{NT1}$ cell line. In mice that were treated, the BPH1 cells underwent malignant transformation, and cells were isolated from the resulting tumor at different time points. After 2 months, a small, non-metastatic tumor had formed (isolated cells became the $BCaP^{T1}$ cell line), and after 4 months a large metastatic tumor had formed (isolated cells from became the $BCaP^{T10}$ cell line, and isolated cells from metastasis site became the $BCaP^{M1}$ cell line). Finally, a $BCaP^{T10}$ xenograft was re-implanted a mouse that was not treated with testosterone and estradiol (castrate conditions); this tumor again metastasized, and cell isolated in the system because the $BCaP^{MT10}$ cell line[2]. LNCaP and derivatives were obtained from collaborators at UW-Madison, and Dr. Donald Vander Griend at the University of Illinois-Chicago generously provided LAPC4 and derivatives. BCaP and LNCaP cell lines were maintained in RPMI 1640+L-glutamine medium (Hyclone, Logan, UT) supplemented with 5% fetal bovine serum (FBS) (Hyclone), 2.5% HEPES (Hyclone), 1% penicillin/streptomycin (P/S) (Hyclone), and 0.2% Normacin (Invivogen, San Diego, CA). For low glucose experiments, RPMI 1640 without L-glutamine and phenol red was used as the base medium.

RNA Immunoprecipitation (RIP)

Eight million cells were collected in 1 mL non-denaturing lysis buffer + HALT (Thermo, 87786) and split between control IgG and DDX3 pulldowns. Lysate protein quantification allowed normalization between cell lines, and each sample was brought to a total volume of 480 µL. 60 µL, or 1/8, of each sample was removed to use for normalization to mRNA input. Protein G Dynabeads (Thermo, 10004D) were bound to DDX3 or IgG control antibodies and incubated for 4 hours at 4 °C with 480 µL of lysate. RNA from each sample, including the input samples, was isolated using Qiagen RNAeasy Mini kit (Cat. No. 74104). cDNA was reversed transcribed from the isolated RNA for input, control, and DDX3 RIP samples as described above, and qPCR (quantitative-PCR) was used to determine mRNA binding targets including AR. qPCR was also run for positive controls CCNE1 and Rac1, and negative control α-tubulin (**supplemental table 2**).

RIP Analysis

All RIP analysis was performed based on the Sigma Imprint Analysis Calculations. ΔCt was calculated for both control (IgG) and experimental (DDX3) samples by subtracting the "input" values from the RIP Ct values. This calculation accounts for RNA sample preparation differences, and differential baseline expression of mRNA targets. The "input" was calculated using the formula: Ct[input] - log2[input dilution factor], where the input dilution factor is 8. The result of subtracting the input Ct from the RIP Ct (for DDX3 and IgG) is the normalized RIP Ct values for each sample. Using the normalized RIP Ct values, we can calculate the ΔΔCt to normalize for non-specific background, which is

defined as: ΔΔCt = ΔCt DDX3 RIP – ΔCt IgG RIP. The fold enrichment of the mRNA target for each sample is calculated using the formula: Fold enrichment = 2^ -ΔΔCt.

Bioanalyzer RNA Visualization and Quantitative-PCR (qPCR)

RNA samples collected from the RIP experiments were visualized and quantified using Agilent 2100 bioanalyzer. Input and DDX3 IP samples showed significant presence of RNA, as expected, whereas significant RNA species in the IgG control pull downs were not present. For qPCR, RNA was isolated using the Maxwell 16 LEV simplyRNA Purification kit (Promega, AS1270), and cDNA was made using iScript Reverse Transcription Supermix (BioRad, 1708841). qPCR for AR and PSA was performed using SSO Universal SYBR (BioRad, 1725271), and data is represented as ΔΔCT, or relative normalized expression. Normalization was calculated in reference to two validated housekeeping genes, TBP and YWHAZ (all primers detailed in **supplemental table 2**), and relative expression was calculated as a fold change of expression compared to the control group.

Cycloheximide Pulse Chase

To determine the degradation rate of AR, cell line models were treated with cycloheximide and expression of AR was determined by Western blot densitometry using ImageJ at 0, 6, and 24 h post-CHX treatment. Poly-ubiquitin was used as a visual control to ensure the cycloheximide treatment is inhibiting translation. As previously described, because poly-ubiquitin binds proteins to mediate degradation, one would expect a decrease of overall polyubiquitinated proteins when translation is decreased[3]. Here, we see that treatment with cycloheximide decreases overall prevalence of

polyubiquitinated proteins, as expected. α-tubulin was used as a loading control. AR protein expression fold change (FC) was determined relative to the 0 h time point.

Tissue Microarrays (TMA)

Both TMAs were acquired from the Prostate Cancer Biorepository Network (PCBN). Dr. Johnathan Melamed collected the CRPC TMA samples at the NYU School of Medicine (IRB #8723). This TMA contains 56 hormone naïve and resistant cores, with the 4 cores per patient (n = 14). Before quantification, tissue quality was assessed resulting in the exclusion of cores with extensive tissue loss or <100 epithelial cells, resulting in final samples sizes of n = 7 hormone naïve and n = 14 hormone resistant. The LuCaP PDX TMA (PCBN 89A-D) was created at the University of Washington by Dr. Colm Morrissey and contains 41 PDXs (patient derived xenografts) with 9 cores per xenograft. These PDXs include CRPC subtypes AR+ (n = 5), AR low/- (DNPC, ARLPC) (n = 3), and NEPC (n = 4). LuCaP35, 23.1, 73, 77, and 96CR represent AR+ CRPC[4,5], LuCaP176, 173.2A, and 173.2B represent AR low/- CRPC (DNPC, ARLPC)[6,7], and LuCaP93, 145.1, 145.2, and 173.1 represent NEPC[8].

Antibodies and immunoblot assays

All antibodies used in the study are detailed in **supplemental table 1**. Western blot (WB) analysis was performed as previously described[9]. Briefly, 30 µg of protein was loaded in each well and primary antibodies including AR, AR D6F11, and DDX3 were detected using a chemiluminescent substrate with α-tubulin used as a loading control.

Multiplexed Immunohistochemistry (IHC)

Immunohistochemistry was performed according to Biocare Medical's protocol, as previously described[10]. For the TMAs, DDX3 was detected with DAB and AR C-terminal was detected with Immpact Red, and counterstained with hematoxylin. Single stained slides were used to create a spectral library for the chromogens, and analysis was done using Vectra automatic image acquisition and InForm 1.4 software as previously described[11]. Briefly, a spectral library is created for each chromogen individually, allowing the optical separation of chromogens during analysis. The method has been validated and utilized in a number of publications[10,12-15]. Segmentation of cellular compartments was done using hematoxylin (nuclear stain) as a marker for nuclei, followed by image "training" in which the software creates an algorithm to identify nuclei in images outside the training set. Visual representations of accurate tissue and cell compartment segmentation are shown in **supplemental figure S1**. For multiplexed fluorescent IHC of MT10 and C42 xenografts, AR C-terminal was incubated overnight (ON) at 4 °C, followed by GαM-HRP and tyramide signal amplification (TSA) 647 (Thermo, B40958). After TSA, the tissue was decloaked for 5 min at 110 °C in citrate buffer and blocked in 2.5% normal horse serum (NHS). DDX3 and PABP1 were incubated for 1 hour at room temperature (RT), followed by secondary antibody DαR-488 for DDX3 and DαM-555 PABP1. Nuclei were counterstained using DAPI.

RNAscope

RNAscope protocol was performed according to ACD Bio recommendations. Briefly, tissues were rehydrated with xylenes and ethanol, and antigen retrieval was performed in the Decloaker with 1X ACD target retrieval buffer. 100 µL of AR RNA probe was incubated at 40 °C for 2 hours. Sequential additions of AMP 1-6 buffers were added

according to ACD Bio's protocol, followed by DAB for 5 min. Nuclei were counterstained with hematoxylin. Staining was quantified using CellProfiler in ImageJ, as previously described[16]. Briefly, each cell is given a positivity score where "0" indicates <1 dot/10 cells, "1" indicates 1-3 dots/cell, "2" indicates 4-9 dots/cell, "3" indicates 10-15 dots/cell, and "4" indicates >15 dots/cell.

Immunofluorescence

Cells were grown on coverslips for 24 hours, fixed with methanol, and permeabilized using 0.25% triton X-100 in phosphate buffered saline (PBS). Cells were blocked in NHS for 1 hour and incubated in primary antibodies overnight at 4 °C. Primary antibodies used were DDX3, PABP1, AR C-terminal, AR N-terminal, Ki67, and cCASP3 (**supplemental table 1**). Secondary antibodies DαR-488 and/or DαM-555 were incubated on the cells for 1 hour at RT. Nuclei were counterstained with DAPI and imaged using a fluorescent microscopy.

DDX3 Vector Overexpression

Overexpression was achieved by transient transfection of a pcDNA-DDX3+YFP plasmid using TransIT-X2 (Mirus, MIR6000) reagent according to MirusBio protocol. Briefly, cells were grown in 6-well plates and transfected with 1 µg vector control or 1 µg pcDNA-DDX3+YFP for 12 hours. After transfection, cells were fixed, permeabilized, and stained for DDX3 and AR N-terminal as described above.

DDX3 Inhibition

Genetic inhibition of DDX3 was achieved by transfection with siRNA targeting DDX3. SMARTpool ON-TARGETplus Human *DDX3X* siRNA (Dharmacon, L-006874-02-0005), with the associated siRNA non-targeting scramble control (Dharmacon, D-001810-10-05). Cells were transiently transfected using Mirus Bio TransIT X2 Dynamic Delivery System (Cat. No. MIR 6005) with either 25 nM siDDX3 or siSCBL control. DDX3 was inhibited pharmacologically using 2 µM RK33 (Selleck Chem, S8246) diluted in DMSO for 48 hours.

MTT Assay

Cells were plated in a 96-well plate at a seeding density of 4000 cells per well, and grown in full media for 24 hours. Cells were then treated one of the following treatments: DMSO control (48 hours), 10 µM bicalutamide (Sigma-Aldrich B9061) or 1 µM enzalutamide alone (24 hours), 2 µM RK33 alone (48 hours), or 2 µM RK33 for 48 hours, with bicalutamide/enzalutamide added after 24 hours. After treatment, cells were incubated in 20 µL MTT diluted to 5 mg/mL in sterile PBS for 1-2 hours at 37 °C. When precipitate formed, the MTT reaction was quenched with 100 mL DMSO, and absorbance was read at 550nm.

Kidney Capsule Xenografts

MT10 and C42 cells were grown to 80% confluence under normal growth condition, and grafts were made with 350,000 cells plus rat tail collagen. The cells were xenografted into the kidney capsule of intact Nu/Nu male mice. In half of the mice, a 25 mg bicalutamide pellet, with cholesterol (CHO), was inserted subcutaneously after 2 weeks. Three days later, DMSO/RK33 injections began, creating four treatment groups: control

(CHO+DMSO), BICA only (BICA+DMSO), RK33 only (CHO+sRK33), and co-treatment (BICA+RK33) with n = 4-6. RK33 injections were given at 20 mg/mL in 0.6% DMSO six times over the course of 2 weeks, as previously described[17,18]. Three days after the last RK33 injection, the mice were euthanized by CO_2, and the tumors were harvested.

Statistics

Bar graphs represent the sample mean with error bars for the standard error of the mean. GraphPad/Prism™ version 7.05 (GraphPad Software, Inc., La Jolla, CA) was used for all statistical analysis with a Student's t-test for comparison of 2 samples, or a one-way ANOVA with Tukey's test for multi-comparison statistics. Significance is represented by * *P*-value ≤ 0.05, ** *P*-value ≤ 0.01, *** *P*-value ≤ 0.001, **** *P*-value ≤ 0.0001.

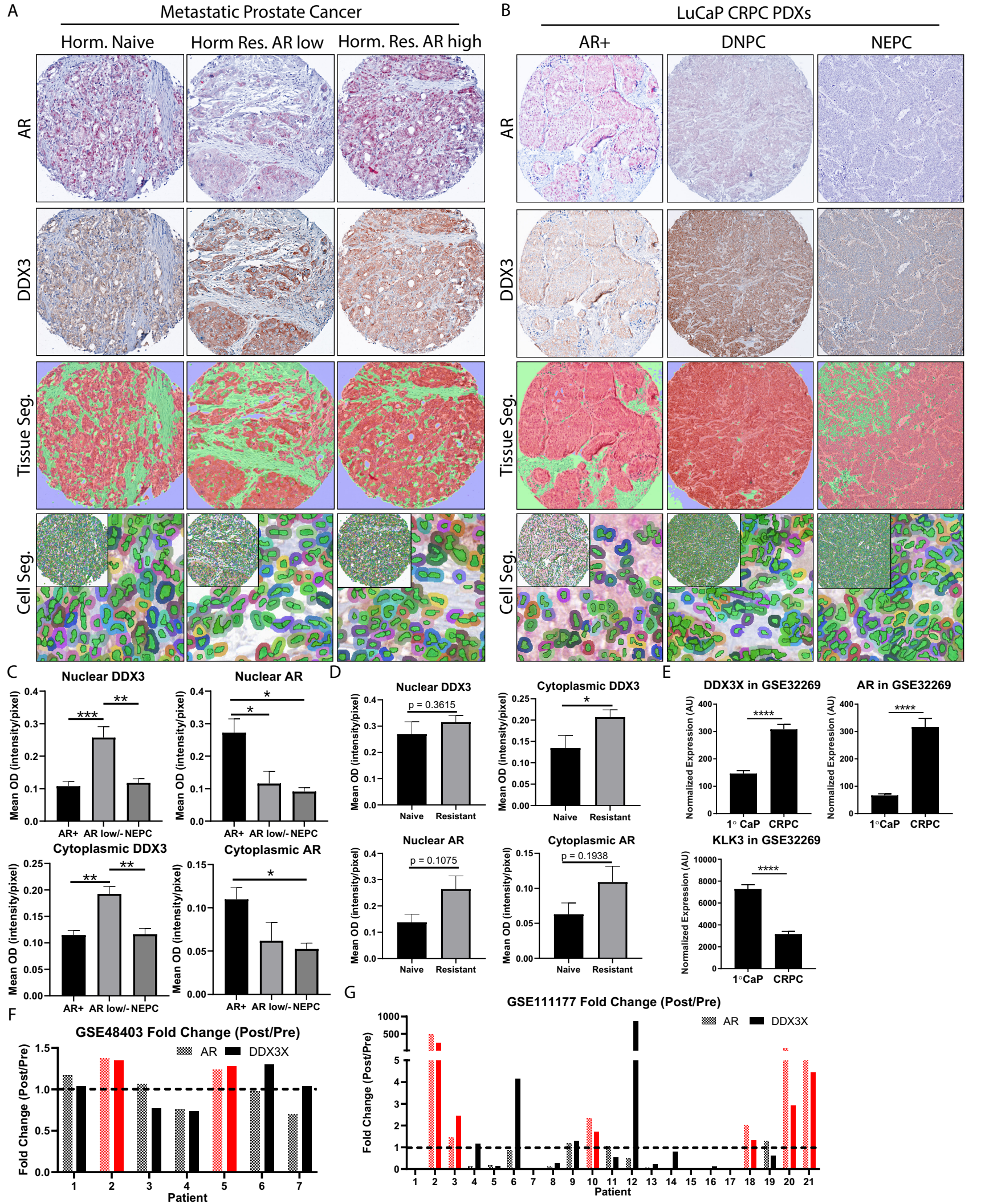
A
Metastatic Prostate Cancer
Horm. Naive
Horm Res. AR low
Horm. Res. AR high
AR
DDX3
Tissue Seg.
Cell Seg.
B
LuCaP CRPC PDXs
AR+
DNPC
NEPC
C
Nuclear DDX3
Nuclear AR
Cytoplasmic DDX3
Cytoplasmic AR
Mean OD (intensity/pixel)
AR+
AR low/-
NEPC
D
Nuclear DDX3
p = 0.3615
Cytoplasmic DDX3
Nuclear AR
p = 0.1075
Cytoplasmic AR
p = 0.1938
Naive
Resistant
E
DDX3X in GSE32269
AR in GSE32269
KLK3 in GSE32269
Normalized Expression (AU)
1°CaP
CRPC
F
GSE48403 Fold Change (Post/Pre)
AR
DDX3X
Fold Change (Post/Pre)
Patient
G
GSE111177 Fold Change (Post/Pre)
AR
DDX3X
Fold Change (Post/Pre)
Patient

Figure S1. InForm software tissue/cellular segmentation and meta-data. (A) Representative images of IHC co-staining for AR (red, first row) and DDX3 (brown, second row) in hormone naïve and hormone resistant (CRPC) specimens. Nuclei were counterstained with hematoxylin (blue). InForm software was trained to segment expression between the epithelial (red) and stromal (green) compartments (third row), and between nuclear (green) and cytoplasmic (multi-colored) cell segmentation (fourth row). **(B)** Representative images of IHC co-staining for AR (red, first row) and DDX3 (brown, second row) in LuCaP PDX samples containing AR+, ARL/- (DNPC, ARLPC), and NEPC subtypes. Nuclei were counterstained with hematoxylin (blue). InForm software was trained to segment expression between the epithelial (red) and stromal (green) compartments (third row), and between nuclear (green) and cytoplasmic (multi-colored) cell segmentation (fourth row). **(C)** Mean optical density of epithelial DDX3 and AR protein expression from the hormone-naïve/resistant samples. n = 7 hormone-naïve, n = 14 hormone-resistant. **(D)** Mean optical density of epithelial DDX3 and AR expression from LuCaP PDX samples. n = 5 AR+ PDXs, n = 3 ARL/- (DNPC, ARLPC) PDXs, n = 4 NEPC PDXs. **(E)** Gene expression analysis of GSE32269 meta-data showed DDX3X and AR mRNA significantly increased in CRPC (n = 29) compared to primary CaP (n = 22) ($P < 0.0001$), while KLK3 (PSA) significantly decreased ($P < 0.0001$). **(F)** Gene expression analysis of GSE48403 showed concurrent increase of AR and DDX3 expressions in post-treatment vs. pre-treatment in two out of the seven patients (28.6%). **(G)** In GSE111177, concurrent increase of AR and DDX3 expressions in post-treatment vs. pre-treatment occurred in 6 out of the 21 patients (28.6%).

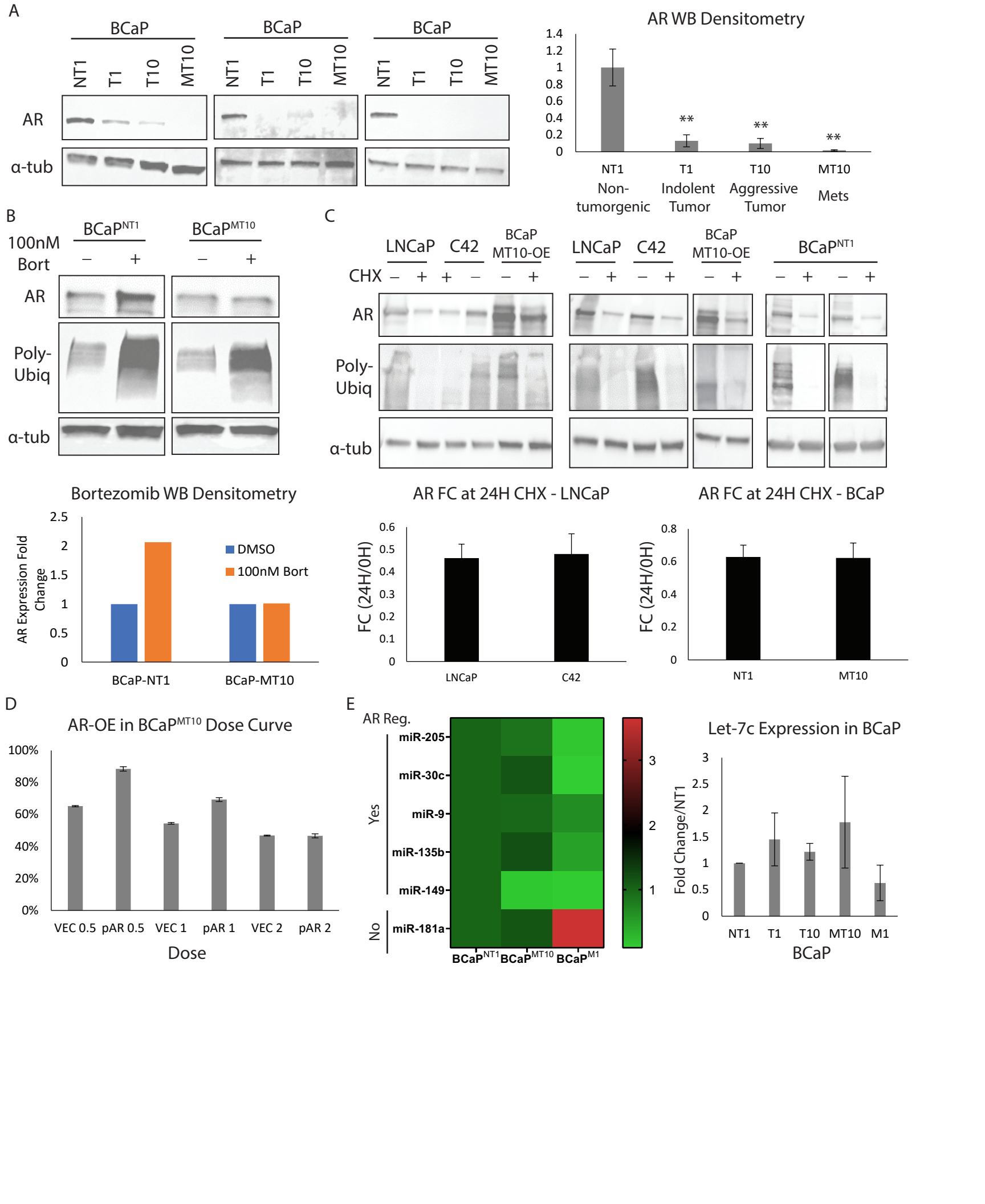
A
BCaP
BCaP
BCaP
NT1
T1
T10
MT10
AR
α-tub
AR WB Densitometry
1.4
1.2
1
0.8
0.6
0.4
0.2
0
**
**
**
NT1
T1
T10
MT10
Non-tumorgenic
Indolent Tumor
Aggressive Tumor
Mets
B
100nM Bort
BCaP^NT1
BCaP^MT10
AR
Poly-Ubiq
α-tub
C
LNCaP
C42
BCaP MT10-OE
LNCaP
C42
BCaP MT10-OE
BCaP^NT1
CHX
AR
Poly-Ubiq
α-tub
Bortezomib WB Densitometry
AR Expression Fold Change
2.5
2
1.5
1
0.5
0
DMSO
100nM Bort
BCaP-NT1
BCaP-MT10
AR FC at 24H CHX - LNCaP
FC (24H/0H)
0.6
0.5
0.4
0.3
0.2
0.1
0
LNCaP
C42
AR FC at 24H CHX - BCaP
FC (24H/0H)
0.8
0.6
0.4
0.2
0
NT1
MT10
D
AR-OE in BCaP^MT10 Dose Curve
100%
80%
60%
40%
20%
0%
VEC 0.5
pAR 0.5
VEC 1
pAR 1
VEC 2
pAR 2
Dose
E
AR Reg.
Yes
No
miR-205
miR-30c
miR-9
miR-135b
miR-149
miR-181a
3
2
1
BCaP^NT1
BCaP^MT10
BCaP^M1
Let-7c Expression in BCaP
Fold Change/NT1
3
2.5
2
1.5
1
0.5
0
NT1
T1
T10
MT10
M1
BCaP

Figure S2. Analysis of AR degradation and miR expression in CRPC models. (A) Western blot replicates for AR protein expression in BCaP cell line model, with α-tubulin used as a loading control. **(B)** Western blot analysis of AR protein accumulation after inhibition of the 26S proteasome by treatment with bortezomib. In $BCaP^{NT1}$ AR protein accumulated, as expected, after treatment with bortezomib (AR blot exposure = 30 sec.). In $BCaP^{MT10}$ AR did not accumulate after treatment with bortezomib, suggesting increased rates of degradation were not contributing to the discrepancy between mRNA and protein expression of AR in this context (AR blot exposure = 300 sec.). Poly-ubiquitin (Ubiq.) was used as the positive control and β-actin was used as a loading control. Bar graphs represent quantification of Western blots by densitometry using ImageJ. **(C)** Western blot replicates for cycloheximide pulse-chase assays to assess AR protein degradation. Poly-ubiquitin was used as a visual control to ensure the cycloheximide treatment is inhibiting translation, and α-tubulin used as a loading control **(D)** Cell viability/proliferation assessed by MTT assay after AR overexpression in MT10. Dose curve shows highest proliferation after transfection with 0.5 µg/mL expression vector for AR. Empty vector represented as VEC, and AR-OE vector represented as pAR. Percent proliferation was calculated based on MT10 doubling time as assessed by MTT. **(E)** Heat map representing expression of a panel of microRNAs (miR) across BCaP progression showed no significant change in expression levels for miRs that have been identified as regulators of *AR* mRNA. miR-181a does not regulate *AR*, but has been shown to increase in BCaP progression, and was used here as a positive control. qPCR analysis showed miR *let-7c* expression was not significantly changed across progression in the BCaP model.

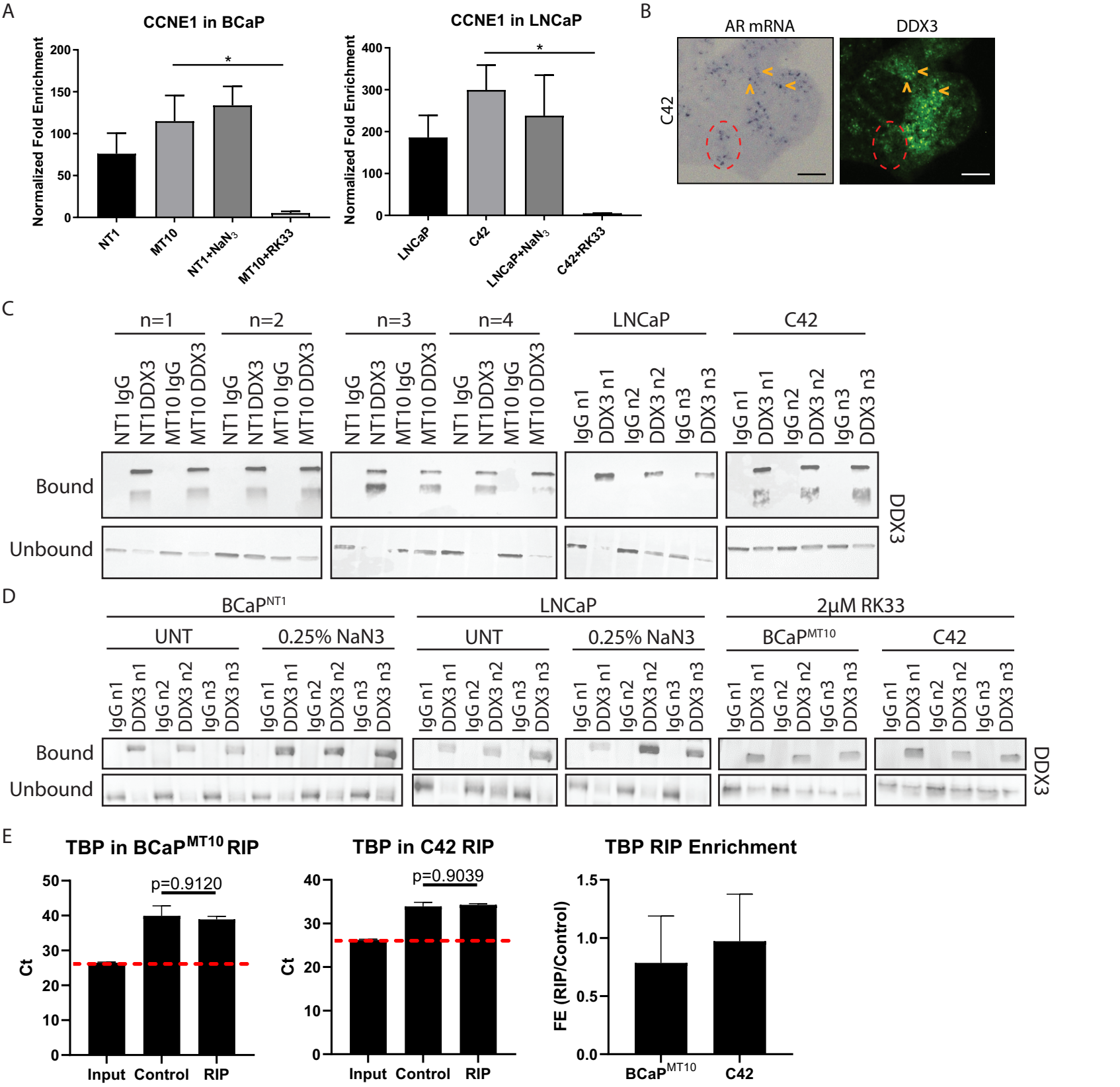
A
CCNE1 in BCaP
Normalized Fold Enrichment
200
150
100
50
0
*
NT1
MT10
NT1+NaN3
MT10+RK33
CCNE1 in LNCaP
Normalized Fold Enrichment
400
300
200
100
0
*
LNCaP
C42
LNCaP+NaN3
C42+RK33
B
AR mRNA
DDX3
C42
C
n=1
n=2
n=3
n=4
LNCaP
C42
NT1 IgG
NT1DDX3
MT10 IgG
MT10 DDX3
IgG n1
DDX3 n1
IgG n2
DDX3 n2
IgG n3
DDX3 n3
Bound
Unbound
DDX3
D
BCaPNT1
LNCaP
2μM RK33
UNT
0.25% NaN3
BCaPMT10
C42
IgG n1
DDX3 n1
IgG n2
DDX3 n2
IgG n3
DDX3 n3
Bound
Unbound
DDX3
E
TBP in BCaPMT10 RIP
p=0.9120
Ct
50
40
30
20
10
0
Input
Control
RIP
TBP in C42 RIP
p=0.9039
Ct
40
30
20
10
0
Input
Control
RIP
TBP RIP Enrichment
FE (RIP/Control)
1.5
1.0
0.5
0.0
BCaPMT10
C42

Figure S3. Analysis of DDX3:AR mRNA complexes by RIP and ISH. (A) RNA-immunoprecipitation (RIP) using DDX3 followed by qPCR for positive control CCNE1 showed binding of DDX3 to CCNE1 mRNA in all cell lines/conditions except with DDX3 inhibition by RK33. **(B)** *In situ* hybridization for AR mRNA (purple) followed by IF for DDX3 (green) demonstrated in some instances, AR mRNA co-localized with DDX3 protein in C42 (yellow arrows); however, steric hindrance from chromogenic amplification of DDX3 may have precluded the binding of the AR mRNA ISH oligos, resulting in an under-representation of co-localization in this assay (dashed red circle). Scale bar = 5 µm. **(C)** Western blot controls for DDX3 RIP analyses in BCaP and LNCaP-C4 series (n = 3) after IP, as previously described. **(D)** Western blot controls for DDX3 in $BCaP^{NT1}$ and LNCaP with NaN_3 treatment (n = 3) after IP, and $BCaP^{MT10}$ and C42 with RK33 treatment (n = 3), as previously described. **(E)** QPCR for negative control Tata-binding protein (TBP) transcripts from DDX3-RIP pull downs in $BCaP^{MT10}$ and C42, where TBP is present in the input samples at a Ct value ~26, but not pulled down in either the IgG control or DDX3 RIP samples. The fold enrichment (FE) for TBP pull down in RIP/control is not significantly different from 1 (i.e. no enrichment) in both $BCaP^{MT10}$ and C42.

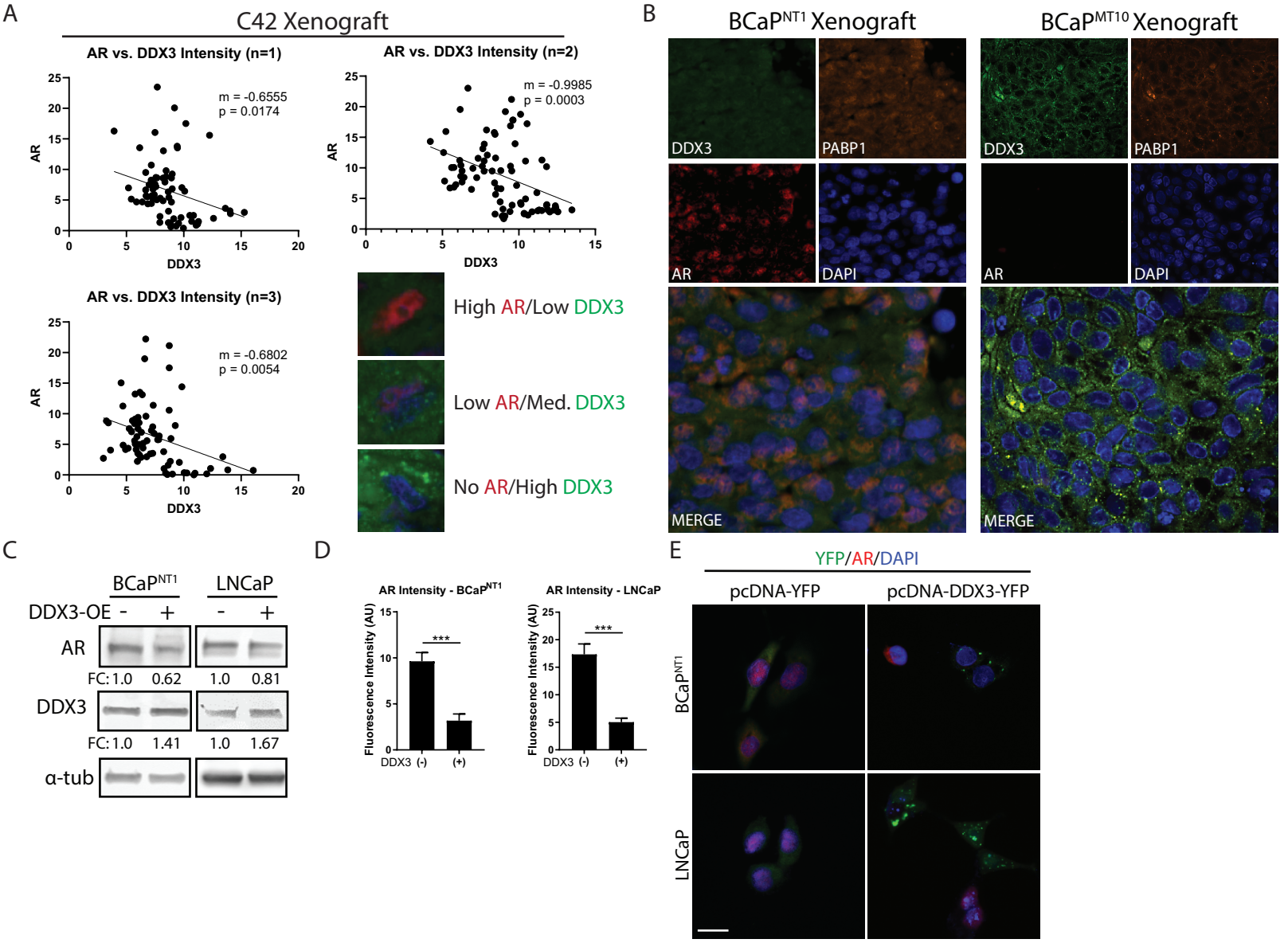
A
C42 Xenograft
AR vs. DDX3 Intensity (n=1)
m = -0.6555
p = 0.0174
AR vs. DDX3 Intensity (n=2)
m = -0.9985
p = 0.0003
AR vs. DDX3 Intensity (n=3)
m = -0.6802
p = 0.0054
AR
DDX3
High AR/Low DDX3
Low AR/Med. DDX3
No AR/High DDX3
B
BCaP^NT1 Xenograft
BCaP^MT10 Xenograft
DDX3
PABP1
AR
DAPI
MERGE
C
BCaP^NT1
LNCaP
DDX3-OE - + - +
AR
FC: 1.0 0.62 1.0 0.81
DDX3
FC: 1.0 1.41 1.0 1.67
α-tub
D
AR Intensity - BCaP^NT1
AR Intensity - LNCaP
Fluorescence Intensity (AU)
***
DDX3 (-) (+)
E
YFP/AR/DAPI
pcDNA-YFP
pcDNA-DDX3-YFP
BCaP^NT1
LNCaP

Figure S4. DDX3 and AR protein expression and negatively associated in CRPC models. (A) Linear regression for DDX3 and AR protein fluorescence intensity in C42 xenografts showed a significant negative correlation between DDX3 and AR expression (n=3). Representative images of single cells from this staining show the spectrum of AR (red) and DDX3 (green) expression levels within the tissue. **(B)** IHC of $BCaP^{NT1}$ and $BCaP^{MT10}$ xenografts grown *in vivo* where DDX3 is shown in green, PABP1 is shown in orange, and AR is shown in red. Nuclei were counterstained with DAPI (blue). **(C)** Western blot analysis of AR protein expression in a bulk population after DDX3 overexpression (DDX3-OE) showed a subtle decrease of overall AR protein (fold change, FC = 0.62 for $BCaP^{NT1}$, and 0.81 for LNCaP) and increase of DDX3 protein (fold change, FC = 1.41 for $BCaP^{NT1}$, and 1.67 for LNCaP). The transfection efficiency for $BCaP^{NT1}$ was around 35%, while the efficiency in LNCaP was only 15%; these low transfection efficiencies may contribute to the subtlety of the effect on AR expression in the bulk population. **(D)** At the single cell level, quantification of AR protein in cells that overexpressed DDX3 (DDX3 +) vs. control vector (DDX3 -) showed significantly decreased AR intensity ($BCaP^{NT1}$ $P = 0.0001$; LNCaP $P = 0.0004$). Fluorescence intensity was averaged between at least 3 separate experiments. **(E)** Representative images of DDX3 overexpression (green) showed cytoplasmic punctate localization that was inversely associated with AR staining (red) in parental cell lines $BCaP^{NT1}$ and LNCaP. Nuclei were counterstained with DAPI (blue).

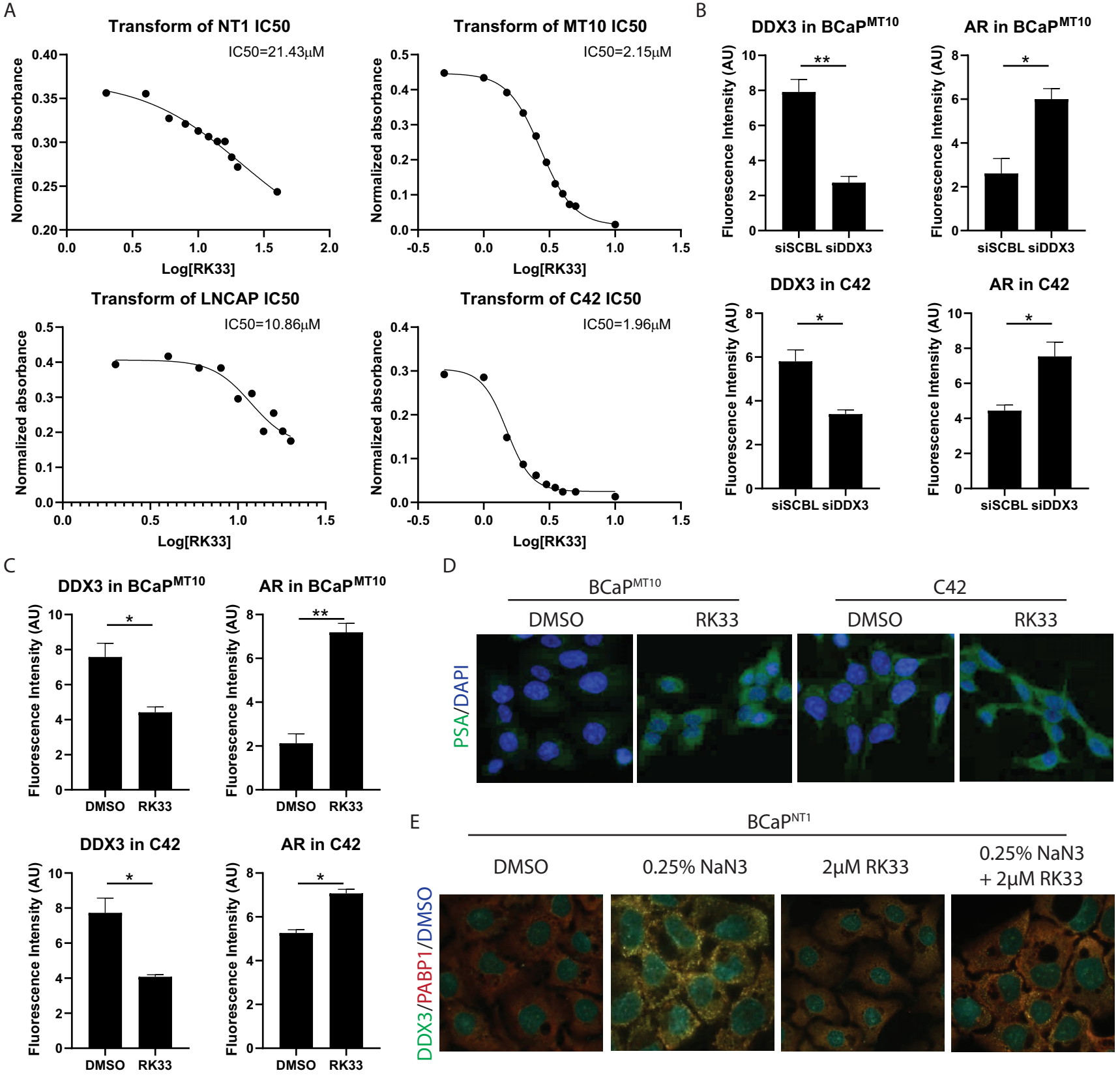
A
Transform of NT1 IC50
IC50=21.43μM
Normalized absorbance
Log[RK33]
Transform of MT10 IC50
IC50=2.15μM
Normalized absorbance
Log[RK33]
Transform of LNCAP IC50
IC50=10.86μM
Normalized absorbance
Log[RK33]
Transform of C42 IC50
IC50=1.96μM
Normalized absorbance
Log[RK33]
B
DDX3 in BCaP^MT10
Fluorescence Intensity (AU)
siSCBL siDDX3
AR in BCaP^MT10
Fluorescence Intensity (AU)
siSCBL siDDX3
DDX3 in C42
Fluorescence Intensity (AU)
siSCBL siDDX3
AR in C42
Fluorescence Intensity (AU)
siSCBL siDDX3
C
DDX3 in BCaP^MT10
Fluorescence Intensity (AU)
DMSO RK33
AR in BCaP^MT10
Fluorescence Intensity (AU)
DMSO RK33
DDX3 in C42
Fluorescence Intensity (AU)
DMSO RK33
AR in C42
Fluorescence Intensity (AU)
DMSO RK33
D
BCaP^MT10
C42
DMSO
RK33
DMSO
RK33
PSA/DAPI
E
BCaP^NT1
DMSO
0.25% NaN3
2μM RK33
0.25% NaN3
+ 2μM RK33
DDX3/PABP1/DMSO

Figure S5. DDX3 inhibition *in vitro* affects AR protein expression and signaling. **(A)** Dose curves for treatment with RK33 assessed by MTT assay, where the log of an increasing concentration of RK33 was plotted vs. normalized absorbance values from MTT, allowing the calculation of IC50 values ($BCaP^{NT1}$ IC50 = 21.43uM, $BCaP^{MT10}$ IC50 = 2.15 µM, LNCaP IC50 = 10.86 µM, and C42 IC50 = 1.96 µM). **(B)** Quantification of fluorescence intensity of DDX3 and AR protein with DDX3 inhibition by siRNAs. Compared to scramble controls, siDDX3 was sufficient to significantly decrease DDX3 protein expression in $BCaP^{MT10}$ ($P = 0.008$) and C42 ($P = 0.032$), while AR protein expression was significantly increased with siDDX3 in both models ($BCaP^{MT10}$ $P = 0.019$; C42 $P = 0.049$). **(C)** Quantification of fluorescence intensity of DDX3 and AR protein with DDX3 inhibition by treatment with RK33. Compared to DMSO controls, RK33 was sufficient to significantly decrease DDX3 protein expression in both models ($BCaP^{MT10}$ $P = 0.043$; C42 $P = 0.047$), while AR protein expression was significantly increased with RK33 ($BCaP^{MT10}$ $P = 0.001$; C42 $P = 0.002$). **(D)** Consistent with KLK3 (PSA) mRNA expression, PSA protein expression was significantly increased when DDX3 was inhibited with RK33. **(E)** Stress granules were induced using sodium azide, followed by inhibition of DDX3 with RK33. DDX3 (green) and PABP1 (red) localized to cytoplasmic puncta when treated with sodium azide alone. With RK33 treatment, DDX3 expression is decreased, and PABP1 expression remains high, but no longer localizes to cytoplasmic puncta, supporting the role of DDX3 as a SG-nucleating factor.

Vellky et al., Figure S6

A

Cancer Type	DDX3X Mutations
Adenocarcinoma	17/3970 (0.45%)
NEPC	0/44 (0.0%)
CRPC	0/70 (0.0%)

B

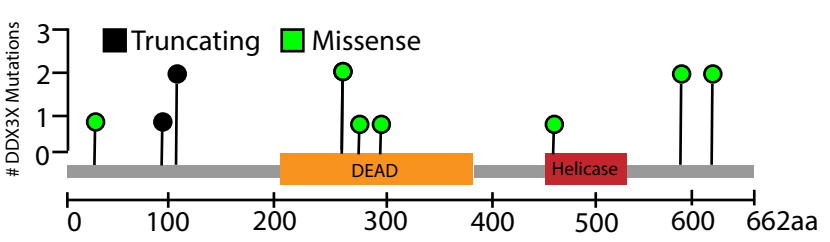

C

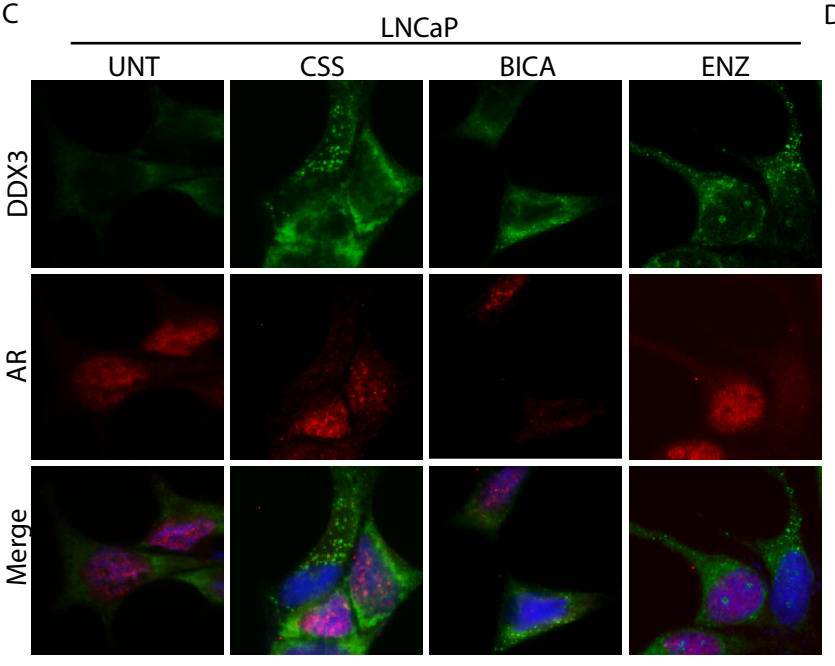

D

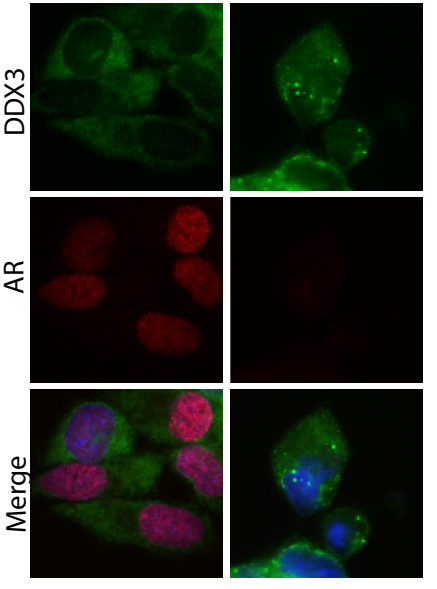

Figure S6. DDX3 localizes to SGs in CRPC in low glucose and low androgen conditions. (A) Interrogation of TCGA cBio portal for mutations in DDX3X showed few mutations in across cancer types. Data was mined by selecting all “prostate” datasets available, selecting “mutation” inquiry, and entering DDX3X as the gene of interest. The mutation data was then segregated by cancer type using the “cancer type detailed” function. There were 17/3970 (0.45%) mutations in adenocarcinomas, 0/44 mutations in NEPC, and 0/70 mutations in CRPC. **(B)** A line plot shows the location within the DDX3X gene that the 17 mutations occurred, and how frequently this location was mutated. **(C)** DDX3 punctate localization (green) is inversely associated with AR protein expression (red) under a variety of conditions including low glucose and ARSI using two clinically relevant anti-androgens (BICA and ENZ). Nuclei were counterstained with DAPI (blue). **(D)** Enzalutamide-resistant LAPC4 cells (LAPC4-ENZr) were derived from the parental line (LAPC4) by constitutive growth in media containing enzalutamide for 6 months, see supplemental methods[19]. These therapy resistant cells show an overall decrease in AR protein (red), and an increase in DDX3 localization to cytoplasmic puncta (green). Nuclei were counterstained with DAPI (blue).

Supplemental Table 1. Commercially available antibody specifics

Antibody	Source	Cat. #	Dilution	Notation
DDX3	Bethyl Laboratories	A300-474A	IHC/IF/RIP 1:250, WB 1:2000	DDX3
AR	Bethyl Laboratories	A303-965A	WB 1:1000	AR
AR	Cell Signaling	5153	WB 1:1000	AR D6F11
AR	Abcam	227678	IHC/IF 1:200, WB 1:1000	AR C-terminal
AR	Santa Cruz	7305	IF 1:100	AR N-terminal
PABP1	Novus Biologicals	120-6125	IHC/IF 1:250, WB 1:1000	PABP1
α-tubulin	Cell Signaling	2144	WB 1:1000	α-tub
Ki67	Abcam	15580	IHC/IF 1:250	Ki67
cCASP3	Cell Signaling	9579	IHC/IF 1:250	cCASP3
Purified Rabbit IgG	Bethyl Laboratories	P120-101	RIP 1:250 (1X)	IgG
Donkey α rabbit 488	Thermo Scientific	A21206	IHC/IF 1:250	DαR-488
Donkey α mouse 555	Thermo Scientific	A31570	IHC/IF 1:250	DαM-555
Goat α Rabbit HRP	Bethyl Laboratories	A120-201P	WB 1:5000	GαR-HRP
Goat α Mouse HRP	Bethyl Laboratories	A90-516P	WB 1:5000	GαM-HRP

Supplemental Table 2. Primers for quantitative PCR analysis

Gene	Size	Primer	Sequence (5'-3')	Length	TM	Location
AR #1	226	Forward	CCAGGGACCATGTTTTGCC	19	61	1628-1646
		Reverse	CGAAGACGACAAGATGGACAA	21	60	1853-1833
AR #2	125	Forward	CAGCCTATTGCGAGAGAGCTG	21	60.87	3313-3333
		Reverse	GAAAGGATCTTGGGCACTTGC	21	59.8	3437-3417
CCNE1	104	Forward	GCCAGCCTTGGGACAATAATG	21	61.3	176-196
		Reverse	CTTGCACGTTGAGTTTGGGT	20	61.1	279-260
PSA	250	Forward	TCATCCTGTCTCGGATTGTG	20	57.03	100-119
		Reverse	ATATCGTAGAGCGGGTGTGG	20	59.04	349-330
YWHAZ	74	Forward	TGATCCCCAATGCTTCACAAG	21	60.3	314-334
		Reverse	GCCAAGGTAACGGTAGTAATCT	22	60.2	389-367
TBP	127	Forward	CCACTCACAGACTCTCACAAC	21	60	366-386
		Reverse	CTGCGGTACAATCCCAGAACT	21	61.8	492-472

Supplemental Table 3. Patient Data for LuCaP TMA Samples

PDX	Anatomic description	Source	Diagnosis	Procedure	AR Protein
LuCaP 173.2A	Metastatic	Rib	DNPC	Autopsy	-
LuCaP 173.2B	Metastatic	Rib	DNPC	Autopsy	-
LuCaP 176	NA	NA	ARLPC	Autopsy	Low
LuCaP 173.1	Metastatic	Liver	Metastatic adenocarcinoma with neuroendocrine differentiation	Autopsy	-
LuCaP 145.2	Metastatic	Lymph node	Metastatic adenocarcinoma with neuroendocrine differentiation	Autopsy	-
LuCaP 145.1	Metastatic	Liver	Metastatic adenocarcinoma with neuroendocrine differentiation	Autopsy	-
LuCaP 93	Primary	Prostate	Adenocarcinoma with neuroendocrine differentiation	Other	-
LuCaP 35	Metastatic	Lymph node	Metastatic adenocarcinoma	Biopsy-Excisional	+
LuCaP 23.1	Metastatic	Lymph node	Metastatic adenocarcinoma	Autopsy	+
LuCaP 73	Primary	Prostate	Adenocarcinoma	Radical prostatectomy	+
LuCaP 77	Metastatic	Bone	Metastatic adenocarcinoma	Autopsy	+
LuCaP 96CR	Primary	LuCaP 96	Adenocarcinoma	PDX	+

PDX = patient-derived xenograft, AR = androgen receptor, NA = not available, DNPC = double negative prostate cancer, ARLPC = AR low prostate cancer.

Supplemental Table 4. Patient Data for Hormone-resistance TMA

Participant ID	Case Type	Surgery Type	Gleason Sum	Length PSA FU (months)	Vital Status	Survival in Years	AR Prot.
1600	Hormone Naïve	TURP	9	23	Dead	1.92	+
1623	Hormone Naïve	TURP	9	73	Dead	6.08	+
1321	Hormone Naïve	TURP	9	11	Dead	1.92	+
1625	Hormone Naïve	TURP	9	116	Dead	18.17	+
1622	Hormone Naïve	TURP	9	18	Dead	2.84	+
1659	Hormone Naïve	TURP	9	67	Dead	12.33	+
1662	Hormone Naïve	TURP	9	3	Dead	0.25	+
1411	Hormone Resistant	TURP	9	11	Dead	0.92	+
1414	Hormone Resistant	TURP	9	59	Dead	4.92	+
1415	Hormone Resistant	TURP	9	0	Dead	13.83	+
1548	Hormone Resistant	TURP	10	3	Dead	0.25	+
1550	Hormone Resistant	TURP	9	11	Dead	0.92	+
1553	Hormone Resistant	TURP	9	26	Dead	2.17	Low
1582	Hormone Resistant	TURP	9	29	Dead	2.42	+
1599	Hormone Resistant	TURP	10	1	Dead	0.08	+
1608	Hormone Resistant	TURP	10	6	Dead	0.5	Neg.
1609	Hormone Resistant	TURP	9	5	Dead	0.42	+
1630	Hormone Resistant	TURP	9	4	Dead	0.33	+
1636	Hormone Resistant	TURP	8	7	Dead	0.58	+
1638	Hormone Resistant	TURP	9		Dead	5.51	+
1660	Hormone Resistant	TURP	9	1	Dead	0.08	Low

TURP = transurethral resection of the prostate, PSA = prostate specific antigen, FU = follow-up, AR = androgen receptor, Neg.= negative

SI References

1. Liu T, Ewald J, Ricke E, Bell R, Collins C, Ricke W. Modeling Human Prostate Cancer Progression in vitro. *Carcinogenesis.* 2018.
2. Vellky JE, Ricke EA, Huang W, Ricke WA. Expression and Localization of DDX3 in Prostate Cancer Progression and Metastasis. *The American Journal of Pathology.* 2019.
3. Hanna J, Leggett DS, Finley D. Ubiquitin depletion as a key mediator of toxicity by translational inhibitors. *Mol Cell Biol.* 2003;23(24):9251-9261.
4. Corey E, Quinn JE, Buhler KR, et al. LuCaP 35: a new model of prostate cancer progression to androgen independence. *The Prostate.* 2003;55(4):239-246.
5. Ellis WJ, Vessella RL, Buhler KR, et al. Characterization of a novel androgen-sensitive, prostate-specific antigen-producing prostatic carcinoma xenograft: LuCaP 23. *Clinical Cancer Research.* 1996;2(6):1039-1048.
6. Lam H-M, Nguyen HM, Labrecque MP, et al. Durable Response of Enzalutamide-resistant Prostate Cancer to Supraphysiological Testosterone Is Associated with a Multifaceted Growth Suppression and Impaired DNA Damage Response Transcriptomic Program in Patient-derived Xenografts. *European urology.* 2019.
7. Bluemn EG, Coleman IM, Lucas JM, et al. Androgen receptor pathway-independent prostate cancer is sustained through FGF signaling. *Cancer cell.* 2017;32(4):474-489. e476.
8. Navone NM, van Weerden WM, Vessella RL, et al. Movember GAP1 PDX project: An international collection of serially transplantable prostate cancer patient-derived xenograft (PDX) models. *The Prostate.* 2018;78(16):1262-1282.
9. Vellky JE, Ricke EA, Huang W, Ricke WA. Expression and Localization of DDX3 in Prostate Cancer Progression and Metastasis. *Am J Pathol.* 2019;189(6):1256-1267.
10. Vellky JE, Bauman TM, Ricke EA, Huang W, Ricke WA. Incidence of androgen receptor and androgen receptor variant 7 coexpression in prostate cancer. *The Prostate.* 2019.
11. Sehgal PD, Bauman TM, Nicholson TM, et al. Tissue-specific quantification and localization of androgen and estrogen receptors in prostate cancer. *Human pathology.* 2019;89:99-108.
12. Sehgal PD, Bauman TM, Nicholson TM, et al. Tissue-specific quantification and localization of androgen and estrogen receptors in prostate Cancer. *Human pathology.* 2019.
13. Nicholson TM, Sehgal PD, Drew SA, Huang W, Ricke WA. Sex steroid receptor expression and localization in benign prostatic hyperplasia varies with tissue compartment. *Differentiation.* 2013;85(4-5):140-149.
14. Bauman TM, Ricke EA, Drew SA, Huang W, Ricke WA. Quantitation of protein expression and co-localization using multiplexed immunohistochemical staining and multispectral imaging. *Journal of visualized experiments: JoVE.* 2016(110).
15. Bauman TM, Vezina CM, Ricke EA, et al. Expression and colocalization of β-catenin and lymphoid enhancing factor-1 in prostate cancer progression. *Human pathology.* 2016;51:124-133.
16. Barriga FM, Montagni E, Mana M, et al. Mex3a marks a slowly dividing subpopulation of Lgr5+ intestinal stem cells. *Cell stem cell.* 2017;20(6):801-816. e807.
17. Xie M, Vesuna F, Tantravedi S, et al. RK-33 radiosensitizes prostate cancer cells by blocking the RNA helicase DDX3. *Cancer research.* 2016;76(21):6340-6350.
18. Bol GM, Vesuna F, Xie M, et al. Targeting DDX3 with a small molecule inhibitor for lung cancer therapy. *EMBO molecular medicine.* 2015;7(5):648-669.

19. Kregel, S., et al. (2016). "Acquired resistance to the second-generation androgen receptor antagonist enzalutamide in castration-resistant prostate cancer." *Oncotarget* **7**(18): 26259-26274.